Integration of Hexagonal Boron Nitride with Quasi-freestanding Epitaxial Graphene: Toward Wafer-Scale, High-Performance Devices

Michael S. Bresnehan,[†,‡] Matthew J. Hollander,[‡,§] Maxwell Wetherington,[†,‡] Michael LaBella,[‡] Kathleen A. Trumbull,[‡] Randal Cavalero,[‡] David W. Snyder,[‡,⊥] and Joshua A. Robinson[†,*]

[†]Department of Materials Science and Engineering, [‡]Electro-Optics Center, [§]Department of Electrical Engineering, and [⊥]Department of Chemical Engineering, The Pennsylvania State University, University Park, Pennsylvania 16802, United States

ABSTRACT

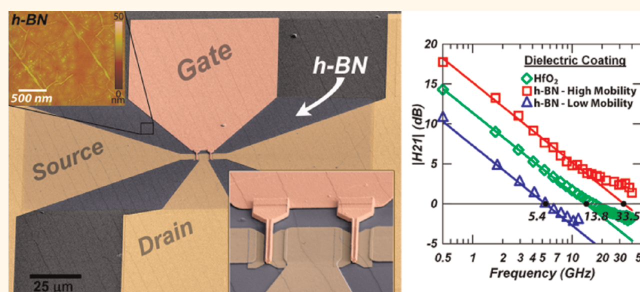

Hexagonal boron nitride (h-BN) is a promising dielectric material for graphene-based electronic devices. Here we investigate the potential of h-BN gate dielectrics, grown by chemical vapor deposition (CVD), for integration with quasi-freestanding epitaxial graphene (QFEG). We discuss the large scale growth of h-BN on copper foil *via* a catalytic thermal CVD process and the subsequent transfer of h-BN to a 75 mm QFEG wafer. X-ray photoelectron spectroscopy (XPS) measurements confirm the absence of h-BN/graphitic domains and indicate that the film is chemically stable throughout the transfer process, while Raman spectroscopy indicates a 42% relaxation of compressive stress following removal of the copper substrate and subsequent transfer of h-BN to QFEG. Despite stress-induced wrinkling observed in the films, Hall effect measurements show little degradation (<10%) in carrier mobility for h-BN coated QFEG. Temperature dependent Hall measurements indicate little contribution from remote surface optical phonon scattering and suggest that, compared to HfO_2 based dielectrics, h-BN can be an excellent material for preserving electrical transport properties. Graphene transistors utilizing h-BN gates exhibit peak intrinsic cutoff frequencies >30 GHz (2.4× that of HfO_2-based devices).

KEYWORDS: graphene · epitaxial graphene · hexagonal boron nitride · h-BN · CVD · gate dielectric · field effect transistor

Graphene exhibits a unique band structure that allows charge carriers to behave as relativistic particles having zero effective mass.[1,2] Consequently, graphene demonstrates exceptional properties such as high charge carrier mobility[3] and high saturation velocity.[4] Such attributes make graphene a promising candidate for radio frequency (rf) applications.[5,6] However, one of the key limitations to the realization of graphene's full potential comes from its interaction with dielectric interfaces, which act to limit the excellent charge transport properties of graphene.[7−9] Typically, top-gated graphene field effect transistors (GFETs) are fabricated with SiO_2 or one of various high-k gate dielectrics.[9,10] Such dielectrics are usually grown either by atomic layer deposition (ALD)[11−13] or electron-beam physical vapor deposition,[14,15] creating an imperfect electrical interface between graphene and the dielectric. These dielectric interfaces introduce scattering from charged surface states,[16,17] remote impurities,[18] remote surface optical phonons,[19] and substrate roughness,[20] significantly degrading the transport properties of graphene. One promising dielectric for potential integration with graphene is hexagonal boron nitride (h-BN), an insulating isomorph of graphene with a lattice mismatch of approximately 1.7%.[21] Ultrathin films of h-BN have been successfully demonstrated through a catalytic thermal CVD growth process on transition metals such as Rh,[22] Ru,[23] Pt,[23] Ni,[24] Pd,[25] and Cu.[26] These h-BN films can be subsequently transferred to arbitrary substrates by removal of the underlying transition metal substrate *via* various transfer processes. Though it has dielectric properties similar to SiO_2 ($\varepsilon \approx 4$, $V_{Breakdown} \approx 0.7$ V/nm),[27] h-BN has several key advantages. Most notably is an atomically smooth surface, expected to be free of dangling bonds due to its strong in-plane covalent bonding and weak interplanar Van der Wals bonds,[28] combined with high energy surface optical phonon modes.[27] Therefore, compared to other dielectrics, the interface

* Address correspondence to jrobinson@psu.edu.

Received for review March 6, 2012 and accepted April 27, 2012.

Published online April 28, 2012
10.1021/nn300996t

© 2012 American Chemical Society

between graphene and h-BN is expected to exhibit a low density of charge traps and adsorbed impurities and is expected to incorporate less remote surface optical phonon scattering. Indeed, it has been shown that h-BN, as a supporting substrate, can significantly improve the properties of exfoliated and CVD grown graphene compared to SiO_2 and high-k dielectrics.[27,29,30] Recently, h-BN/graphene/h-BN heterostructures have been fabricated and shown to improve transconductance by 70% and increase transistor cutoff frequency by nearly $2\times$ compared to SiO_2-supported, Al_2O_3-gated GFETs.[31] Additionally, the potential for large-scale development has been demonstrated with h-BN integrated as a back-gate dielectric utilizing CVD grown graphene.[32] Although the benefits of h-BN/graphene systems have been demonstrated previously, current focus has been limited to h-BN integration with CVD or exfoliated graphene. The effects of h-BN on epitaxial graphene, which is more conducive to large scale development and commercialization, have not yet been investigated. Epitaxial graphene has been shown to produce uniform, large area, and high quality graphene for high frequency applications with an intrinsic current gain cutoff frequency (f_T) approaching 300 GHz.[33] In addition, epitaxial graphene has recently been further enhanced by hydrogen intercalation, where the interfacial (buffer) layer present in epitaxial graphene is passivated by hydrogen, forming a "quasi-freestanding" epitaxial graphene (QFEG) which leads to mobility improvements of approximately $2.5\times$ and extrinsic f_T improvements of $>3\times$.[34,35]

Here, we demonstrate the *first* 75 mm QFEG wafer with CVD h-BN top-gated GFETs (Figure 1a). Although the catalytic CVD growth of h-BN results in nonuniform surface wrinkling, we show that the h-BN film does not chemically or structurally degrade after transfer and that the removal of the as-grown copper substrate results in a significant relaxation of compressive strain. Electrical characterization indicates that CVD h-BN integration with QFEG results in significantly less remote surface optical phonon scattering and introduces less charged impurities to the system relative to HfO_2 based dielectrics. Additionally, the overall benefit of h-BN relative to HfO_2 dielectrics is found to be critically dependent on the initial mobility of the QFEG samples which results in unique limitations not typically observed in h-BN integration with exfoliated or CVD grown graphene. On *high mobility* QFEG samples (>2000 $cm^2/(V\text{-}s)$) with low carrier and impurity densities, h-BN gate dielectrics are shown to effectively preserve mobilities >3000 $cm^2/(V\text{-}s)$ at room temperature, ultimately leading to intrinsic transistor cutoff frequencies of 33.5 GHz for 750 nm gate lengths. However, for *low mobility* QFEG samples (<1500 $cm^2/(V\text{-}s)$) with high carrier and impurity densities, Coulombic scattering dominates transport and the benefits of h-BN are quenched relative to HfO_2 due to its low dielectric constant.

RESULTS AND DISCUSSION

Chemical vapor deposited h-BN films exhibit high crystalline and chemical quality; however the transfer process presents challenges that must be addressed for optimized device development. Scanning electron microscopy (SEM) of as-grown h-BN on Cu and transferred h-BN on SiO_2 (Figures 1b,c) clearly demonstrates the presence of wrinkles across the film, similar to those observed elsewhere.[36] The wrinkles, also observed with atomic force microscopy (AFM) in Figure 1d, results from the anisotropic thermal expansion of h-BN, where a negative coefficient of thermal expansion (CTE) exists in the plane of bonding.[37] This negative CTE causes the h-BN film to expand during cooling while the copper substrate shrinks, inducing a compressive stress in the h-BN film. This compressive stress results in as-grown film bunching over the Cu step edges (Figure 1b) and local areas of film delamination in the form of wrinkles. Following transfer of the film (Figure 1c,d), the h-BN relaxes over the SiO_2 substrate; however, large wrinkles are still apparent after transfer. These wrinkles were measured with AFM to be approximately 6−10 nm high for 10 nm thick films and increase in height with increasing film thickness. The variation in total film thickness that results from wrinkling presents a challenge to graphene device fabrication, as h-BN wrinkles in the graphene channel will result in a nonuniform electric field. This phenomenon is also observed in transferred CVD grown graphene, where wrinkling is significantly reduced by incorporating an additional PMMA application step following initial transfer in order to relieve stress in the film.[38] Similar modifications to our current process may also benefit from this additional step and provide improved transfer morphology of CVD grown h-BN films.

Raman spectroscopy verifies that the h-BN film experiences a compressive stress during cooling which is partially relaxed upon transfer. Raman was first performed on the as-grown h-BN film on Cu. The same film was then transferred to the QFEG wafer where Raman scans were taken over Hall crosses and over etched regions (bare SiC). The use of the same h-BN film for Raman analysis was critical to rule out effects of thickness variations between different samples. Figure 1e clearly demonstrates a red-shift in peak position from the as-grown (1373 cm^{-1}) to transferred film over SiC (1370 cm^{-1}), where the bulk value of the h-BN E_{2g} phonon mode (ω^0) is located at 1366 cm^{-1}.[39] The Raman E_{2g} peak shift ($\Delta\omega_{E_{2g}}$) provides a means to estimate strain relaxation in the h-BN film upon transfer *via*[40] $\Delta\omega_{E_{2g}} = -2\omega^0\gamma_{E_{2g}}\varepsilon$, where $\gamma_{E_{2g}}$ is the Grüneisen parameter for the Raman-active E_{2g} phonon mode of h-BN ($\gamma_{E_{2g}} = 0.1$)[41] and ε is the strain tensor. Given that

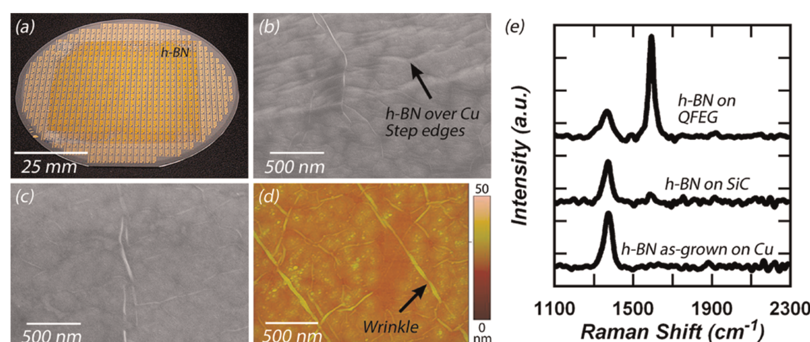

Figure 1. (a) Quasi-freestanding epitaxial graphene transistors fabricated on a 75 mm SiC wafer upon which a 50 mm × 50 mm h-BN sheet is transferred to and subsequently patterned. (b) SEM image of as-grown h-BN on a copper substrate. The h-BN layer conforms to the steps of the Cu substrate, evident by the buckling of the overlying h-BN film. (c) SEM image of the same h-BN film after transfer to a 300 nm thick SiO_2 substrate. The buckling induced from the Cu substrate relaxes over the SiO_2 surface. However the wrinkles, induced from stress during cooling, remain. (d) AFM of h-BN transferred to SiO_2 shows wrinkling of the h-BN sheet. (e) High resolution Raman spectra of as-grown h-BN on the copper substrate compared to transferred h-BN on a SiC substrate and over QFEG.

the as-grown and transferred film is of identical thickness, the shift in the E_{2g} peak may be directly attributed to strain relaxation of h-BN during the transfer process from the as-grown copper substrate to the supporting SiC/QFEG substrate. The stress relaxation (~3 cm^{-1} shift in the E_{2g} peak position) associated with the removal of the Cu substrate corresponds to a 42.3% decrease in compressive strain upon transfer. The overall blue-shifted Raman peaks observed here have also been reported for as-grown atomically thin h-BN films[42] and h-BN nanotubes[43] and are attributed to a hardening of the E_{2g} phonons due to an increase in h-BN's lattice constant from the lack of interaction from neighboring sheets.[43] However, for this study, Raman was performed on multilayer films (approximately 50 nm) to obtain a high intensity Raman signal and to provide pinhole free dielectric layers for device applications. Thus, the upward shift from h-BN's bulk Raman frequency observed here is presumably due to substrate induced compressive stress; although substrate induced charge carrier doping cannot be ruled out. The Raman spectra of the h-BN film over a graphene Hall cross clearly shows the spectral contribution from the under-lying graphene. The E_{2g} phonon mode of graphene, or G-Peak, is apparent at 1591 cm^{-1}. Additionally, a shoulder on the h-BN peak, corresponding to the overlapping D-peak of graphene (attributed to defects in QFEG),[44] is observed at approximately 1355 cm^{-1}. The smaller peaks in the spectral noise are remnants from the background subtraction processing of the raw data.

Evident from X-ray photoelectron spectroscopy (XPS), CVD deposited h-BN is chemically stable during the transfer process. The high resolution B1s and N1s core level peaks (Figure 2a, b) are located at 190.7 and 398.3 eV, respectively, matching reported values for bulk h-BN, which give the N1s peak at 398.1 eV and the B1s peak at 190.1 eV.[45] Additionally, there is no evidence of oxidation and the measured atomic

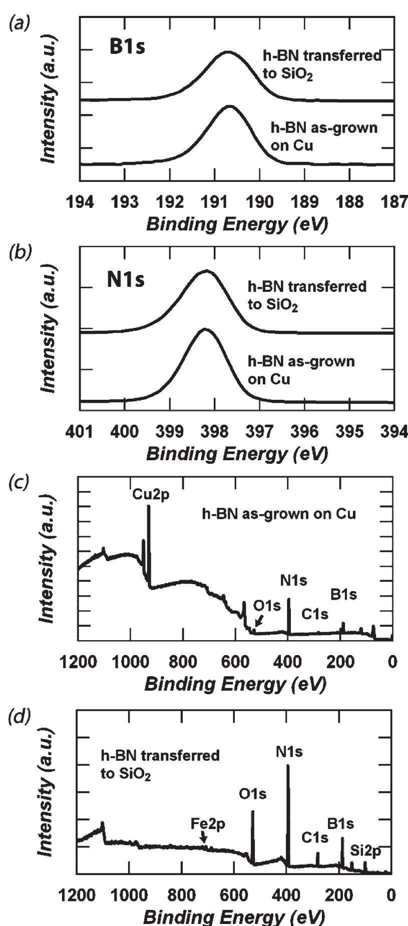

Figure 2. XPS spectra of as-grown h-BN films on copper foil and after transfer to 300 nm SiO_2. (a,b) High resolution XPS spectra of B1s and N1s core level peaks. The peak position of both as-grown and transferred B1s and N1s peaks are similar to literature values, and peak shape indicates no apparent contributions from carbon or oxygen bonding in the h-BN lattice. (c,d) Low resolution XPS survey spectra for as-grown and transferred h-BN. The as-grown film contains very little oxygen and carbon contamination. The transferred h-BN shows a small Fe 2p peak, indicating iron contamination induced from the copper etchant during the transfer process which will likely effect carrier transport in QFEG.

percentages indicate excellent stoichiometry with a B/N ratio of 0.97. Both the B1s and the N1s core level peaks exhibit no shift in peak position or shape after transfer, indicating no modification of chemistry has occurred. The symmetric shape of the as-grown and transferred B1s and N1s peaks provide direct evidence that no carbon−boron or carbon−nitrogen bonding has occurred during synthesis or transfer, unlike previous reports for hybrid h-BN/graphene domains.[46] Therefore, the C1s peak observed in Figure 2c,d is likely due to adventitious carbon. Low resolution XPS spectra of the transferred h-BN film (Figure 2d) also indicates the presence of the Fe 2p peak, which correlates to an iron impurity level of approximately 2 atomic %, presumably located at the h-BN/SiO_2 interface. Residual iron impurities are likely due to the ferric chloride etchant used to remove the Cu substrate during the transfer process. Additionally, silicon and oxygen peaks are due to the SiO_2 substrate utilized in XPS investigations. Nonlabeled peaks in the spectra are secondary peaks of already established elements.

Despite the presence of stress-induced wrinkling observed in AFM and SEM, room temperature Hall effect measurements (Figure 3a) indicate that the carrier mobility and concentration of the QFEG are minimally affected upon integration with the h-BN dielectric overlayer, although this is partially a result of the initial low mobilities inherent to the epitaxial graphene system (~1500 cm^2/V sec at 1×10^{13} cm^{-2}). Upon transfer, the QFEG experiences an average increase in hole concentration of approximately 5×10^{11} cm^{-2} (<5 ± 2%), which is coupled with a 14 (±3)% decrease in average Hall mobility, from 1741 cm^2/(V-s) to 1499 cm^2/(V-s). Hole doping of the graphene is attributed to the presence of residual water at the h-BN/QFEG interface subsequent to h-BN transfer. After a 20 min anneal to remove residual photoresist and water at 400 °C in H_2/N_2 (15% H_2), the carrier concentration returns to as-grown values, which indicates that the h-BN itself does not significantly induce hole doping within the QFEG; however, Hall mobility remains an average of 9 (±5)% below its original value. These results were consistent for h-BN films with thicknesses from 10 to 50 nm indicating that doping induced by the h-BN layer is independent of thickness. The degradation in mobility is attributed mainly to the addition of impurities at the dielectric/graphene interface during the transfer process (such as Fe impurity contamination from the solution transfer process as observed in Figure 2d) which act to increase remote charged impurity scattering within the QFEG.[9,10] Figure 3b plots the temperature-dependent Hall mobility before and after h-BN integration and confirms an increase in remote charged impurity scattering. This is shown by a reduction in the temperature-independent portion of the curve after h-BN integration, which is dominated by remote charged impurity scattering.[47] In another work (not yet published),[48] physics-based

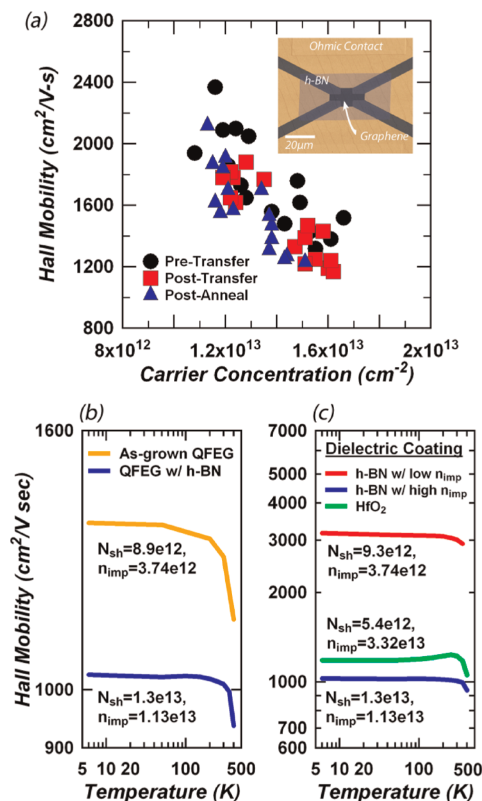

Figure 3. Room temperature Hall mobility *versus* carrier concentration (a) obtained from Van der Pauw test structures before h-BN integration, after h-BN transfer, and after annealing at 400 °C for 20 min in H_2/Ar (15% H_2) shows minimum degradation of the carrier mobility. Inset: SEM micrograph of Van der Pauw test structure after transfer and patterning of h-BN dielectric layer. (b) Hall mobility *versus* temperature before and after h-BN integration shows minimal change in the surface optical scattering as well as the incorporation of additional remote charged impurity scattering. (c) Temperature-dependent Hall mobility shows the potential of h-BN in preserving high mobilities for QFEG due to reduced introduction of charged impurity and remote surface optical phonon scattering compared to HfO_2. Here, N_{sh} is the sheet carrier density (cm^{-2}) and n_{imp} is the approximate remote charged impurity density extracted using techniques adopted from Konar *et al.*[49]

modeling of the temperature-dependent transport data indicates remote charged impurity scattering as the dominant scattering source in these samples and that integration of CVD h-BN can introduce up to 6×10^{12} additional impurities/cm^2 at the dielectric-graphene interface, although this value was found to be roughly 4× less than that introduced by HfO_2 dielectrics and can be as low as 3×10^{12} cm^{-2}. In this way, h-BN integration can be beneficial in reducing the number of additional remote charged impurity scatterers.

Temperature-dependent Hall effect measurements indicate little contribution from remote surface optical phonon scattering after h-BN integration (Figure 3c). For a *high mobility* h-BN coated QFEG samples, exhibiting mobilities greater than 3000 cm^2/(V-s) and with a low impurity density of 3.7×10^{12} cm^{-2}, the ultimate decrease in mobility from the low temperature,

impurity limited regime to the high temperature, phonon limited regime is only 4.4% and can be explained simply as a result of intrinsic phonon scattering within the graphene. The method presented by Konar *et al.*[47] was adapted here to show that for a fixed carrier concentration and charged impurity density of 9.3×10^{12} cm^{-2} and 3.7×10^{12} cm^{-2}, respectively, (given an acoustic deformation potential of 4.8 eV, optical deformation potential of 25.6 eV/A, and intrinsic optical phonon energy of 140 meV) the expected change in mobility due to optical and acoustic phonon scattering from 5−400 K is only 5%, which matches well with our experimental results and indicates that phonon-carrier coupling is extremely limited for the h-BN/graphene system. These results are similar to results published elsewhere for uncoated QFEG samples, which exhibit minimal temperature dependence of Hall mobility and confirm that pristine QFEG samples exhibit minimal remote surface optical phonon scattering from surface modes within the substrate.[49] Importantly, our results show that even with h-BN integration, this limited effect of remote surface optical phonon scattering can be preserved, suggesting that h-BN introduces little additional remote surface optical phonon scattering. Alternatively, for a *low mobility* h-BN coated sample (Figure 3b,c), exhibiting mobilities ~1100 cm^2/(V-s) and with an approximate fixed impurity density of 1.1×10^{13} cm^{-2}, the decrease in mobility was 7.7% for the same temperature range and indicates an increase in remote surface optical phonon scattering for this sample. However, the change in temperature dependence before and after dielectric integration (Figure 3b) is minimal and again indicates that the h-BN introduces negligible additional remote surface optical scattering. Instead, the increased contribution from remote surface optical phonons in both the as-grown and h-BN coated sample is thought to originate from the SiC substrate, where an increased SiC step-edge density was found for this particular sample and is thought to lead not only to a higher density of remote charged impurities, evidenced by the reduction in the temperature independent mobility (remote charged impurity dominated), but also to increased phonon scattering and reduced mobility. Degradation of transport properties with presence of step-edges for epitaxial graphene is a well-known phenomenon and has been reported elsewhere.[50]

In contrast, the HfO-coated QFEG sample exhibits a 14.5% degradation in temperature dependent mobility, which fits well with expected results and verifies that the use of high-k dielectrics induces additional remote surface optical phonon scattering compared to h-BN dielectrics. Modeling of the temperature-dependent data (not shown) indicate that remote surface optical scattering contributes ~15% of the total mobility reduction in these samples. Despite this increase in remote surface optical phonon scattering as well as

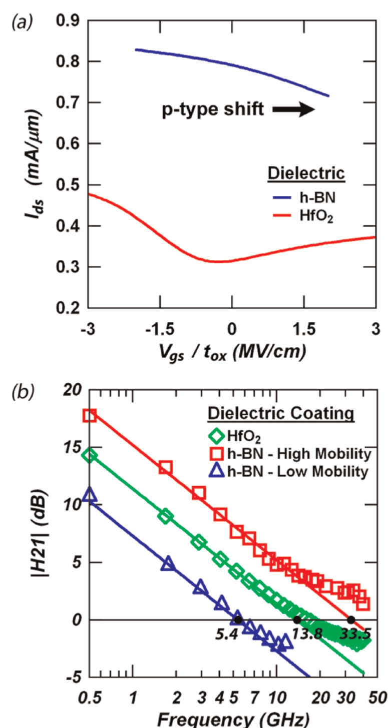

Figure 4. (a) Drain current as a function of gate voltage for h-BN and HfO_2-gated GFETs. The p-type doping of the h-BN-gated GFET shifts the minimum conductivity point in the positive direction while use of an HfO_2 gate leads to a minimum conductivity point close to zero volts. (b) Intrinsic RF performance of h-BN and HfO_2-gated GFETs. For the high mobility QFEG sample with low impurity density, the small degree of remote surface optical scattering from use of h-BN dielectrics leads to excellent RF performance.

remote charged impurity scattering, the ability of the HfO_2 to screen the carriers from remote charged impurities results in an average increase in carrier mobility when initial as-grown mobility is heavily dominated by remote charged impurity scattering.[47] However, for QFEG samples exhibiting a high initial mobility (phonon limited regime), the increased surface optical phonon scattering from HfO_2 results in a large degradation in mobility compared to h-BN. Therefore, QFEG's mobility is limited by HfO_2 for *high mobility* QFEG samples and benefits from HfO_2 for *low mobility* QFEG samples.[10,47] In contrast, the benefit of h-BN is most evident in the *high mobility* QFEG (phonon limited) regime. Additionally, Figure 3c shows a small increase in Hall mobility with temperature for the HfO_2-coated sample before decreasing at higher temperatures. This increase in mobility occurred in conjunction with a decrease in the carrier density and is attributed to the presence of temperature-activated traps in the HfO_2 overlayer which capture charges and lead to an increase in mobility. Similar behavior has been reported for uncoated epitaxial graphene where an increase in Hall density and subsequent decrease in Hall mobility were reported and attributed to donor traps in the SiC substrate.[51]

Electrical characterization of CVD grown h-BN and HfO_2-gated GFETs confirms that the use of h-BN dielectrics can be effective in preserving the transport properties of *high mobility* QFEG samples. Though Britnell *et al*. suggests that exfoliated single-crystal h-BN flakes show negligible tunneling currents at thicknesses of only four layers,[52] CVD h-BN used here resulted in significant leakage currents and $V_{Breakdown} < 1$ V for thicknesses up to 20 nm, which may be a result of pin-holes or nonuniformities in the transferred films. Therefore, for GFET characterization, an h-BN thickness of 50 nm was used to ensure sufficiently low gate leakage currents (measured to be $<1 \times 10^{-10}$ A/μm^2 at $V_{gs} = 1$ V). Figure 4a plots drain current as a function of gate voltage ($V_{ds} = 1$ V) for typical h-BN and HfO_2-gated GFETs and shows the characteristic p-type transfer curve of QFEG graphene for h-BN-gated GFETs, where hole doping of the QFEG is a result of the intrinsic spontaneous polarization charge of the hexagonal SiC substrate.[50] Alternatively, HfO_2-gated GFETs exhibit slightly n-type behavior and V_{Dirac} much nearer to 0 V, which is attributed to n-type doping by the HfO_2 overlayer that competes with the substrate-induced hole doping.[35] The heavily p-type behavior of the h-BN gated devices leads to increased drain currents over the range of evaluated gate voltages compared to HfO_2-gated GFETs. Besides increased drain currents, the shift in transfer curve also leads to reduced transconductance over the same voltage range, evidenced as a decrease in the on−off ratio. Despite this reduction in transconductance, RF performance for h-BN-gated GFETs can be up to 2.4× that of HfO_2-gated GFETs, although ultimate performance is found to be highly dependent on initial mobility of the QFEG sample. Figure 4b plots the small signal current gain for three different GFETs as a function of frequency. The results show that for *low mobility* QFEG, use of h-BN top-gates shows no benefit compared to HfO_2 dielectrics, producing current gain cutoff frequencies of 5.4 GHz (4.05 GHz-μm) compared to 13.8 GHz (10.4 GHz-μm) for HfO_2 coated GFETs, where the significant decrease in RF performance for h-BN coated GFETs is partially attributed to the reduction in transconductance caused by the p-type shift of the transfer curve. Alternatively, for *high mobility* QFEG, use of h-BN leads to cutoff frequencies as high as 33.5 GHz (25.12 GHz-μm), which is the highest $f_T \cdot L_g$ product reported for h-BN-coated graphene transistors and is attributed to a reduced contribution from remote surface optical phonon scattering and a lower density of remote charged impurities relative to HfO_2-coated GFETs that acts to preserve the excellent transport properties of QFEG.

CONCLUSIONS

We have demonstrated the growth of high quality CVD h-BN and its integration as a gate dielectric with quasi free-standing epitaxial graphene-based devices as well as its potential for wafer-scale development. The as-grown h-BN was shown to be of high chemical and crystalline quality, which does not degrade as a result of the transfer process. We have also shown that the h-BN film relaxes significantly from the compressively strained as-grown state upon transfer. Despite the presence of wrinkles on the h-BN surface, the negligible introduction of remote surface optical phonon scattering and remote charged impurity scattering compared to high-k dielectrics allows for the excellent preservation of QFEG's transport properties. However, we have shown that the benefit of CVD h-BN over high-k dielectrics is highly dependent on the initial carrier mobility of the QFEG sample, where remote impurity scattering in low mobility QFEG (high impurity density) can mask the potential benefits of h-BN dielectrics. Alternatively, for high carrier mobility QFEG, h-BN effectively preserves carrier mobility >3,000 cm^2/(V-s) at room temperature and results in intrinsic cutoff frequency improvements of 2.4× over HfO_2-gated QFEG. With improvements in the growth of epitaxial graphene and reduction of impurity contamination from the h-BN transfer process, CVD h-BN may prove to be an excellent dielectric for QFEG and other types of graphene due to its low surface optical phonon scattering contributions.

METHODS

Epitaxial graphene is grown on 75 mm wafers *via* the sublimation of silicon from 6H-SiC (0001) at 1625 °C for 15 min under 1 Torr argon (Ar) background pressure.[53] The wafers are then exposed to 600 Torr hydrogen (H_2) at 1050 °C for 120 min to intercalate hydrogen at the graphene/SiC(0001) interface.[35] Van der Pauw (VdP) Hall crosses and radio frequency field-effect transistor structures are fabricated using standard ultraviolet photolithography. VdP structures are 5 μm × 5 μm squares and often incorporate SiC step edges known to effect carrier density and mobility,[50] while transistors utilize two-finger gates, 2 × (10 × 1 μm^2) ($W \times L$) with 750 nm source-drain spacing. Source/drain contacts (Ti/Au 10/50 nm) were prepared using an oxygen plasma pretreatment, as detailed in previous work.[53]

Hexagonal boron nitride is grown on 99.8% pure Cu foils (Alfa Aesar, part no. 13382) in a 75 mm diameter horizontal tube furnace *via* a catalytic thermal CVD method utilizing a single ammonia borane (NH_3BH_3) precursor (Sigma-Aldrich, part no. 682098) similar to previously reported methods.[54] The Cu foils are cleaned in a heated acetone bath and subsequently annealed at 800 °C, 1 Torr for 20 min under H_2/Ar (15% H_2) flow to remove the native oxide. Solid ammonia borane powder is sublimed at 135 °C and transported into the tube furnace by H_2/Ar carrier gas (5% of total flow rate). Growth occurs at 1050 °C and 250 mTorr with growth times between 5 and

30 min, depending on desired film thickness. After the growth procedure, the ammonia borane carrier gas is turned off and the furnace is allowed to slowly cool to room temperature in a 250 mTorr Ar/H_2 environment.

The as-grown h-BN films are characterized using Raman spectroscopy, atomic force microscopy (AFM), scanning electron microscopy (SEM), and X-ray photoelectron spectroscopy (XPS). A WITec CRM200 Confocal Raman microscope with a 488 nm laser wavelength is utilized for structural characterization. For as-grown h-BN, the Raman background signal due to the copper substrate is subtracted using a best-fit polynomial technique while the h-BN films transferred to QFEG wafers utilize a direct subtraction of the SiC substrate from the spectra. For XPS, SEM, and AFM analysis, 15 mm $\times$ 15 mm h-BN films were transferred to oxidized silicon substrates with an oxide thickness of 300 nm due to the uniform smoothness of SiO_2 relative to SiC, which has step edges that could influence the transferred film morphology. A Digital Instruments Dimension 3100 with a scan rate of 0.8 Hz was utilized for AFM measurements. A Leo 1530 field emission SEM with an accelerating voltage of 5 kV was used to acquire SEM micrographs. A Kratos Axis Ultra XPS system utilizing an Al kα source with energy of 1486 eV was used for XPS analysis. For transfer to SiO_2 and QFEG substrates, the h-BN on Cu films are coated with photoresist (950 PMMA A3) and soft baked at 160 °C for 1 min. The Cu substrate is removed using a ferric chloride solution, similar to previously reported techniques for transfer of CVD grown graphene from Cu.[55] The remaining PMMA/h-BN film is then transferred to a series of water baths to remove residual etchant and subsequently transferred to the final substrate. Electrical evaluations and large area development is accomplished using 50 mm $\times$ 50 mm h-BN films transferred to 75 mm QFEG wafers previously patterned with ohmic level device structures. The PMMA is then removed with acetone and the h-BN/substrate is heated to 50 °C to drive off residual water. Removal of residual PMMA is accomplished *via* a post-transfer anneal at 400 °C for 20 min in an H_2/N_2 (15% H_2) environment. For wafers with graphene devices, the h-BN dielectric layer is patterned and etched with an Applied Materials MERIE using a CHF_4/CF_4 mixture to clear the ohmic contacts of h-BN. Thickness was determined through AFM measurements performed on the edges of the transferred h-BN films. The thickness of the h-BN film is controlled by varying the growth time, where films from a few layers up to 50 nm thick have been grown and successfully transferred to arbitrary substrates. Room temperature Hall measurements of VdP test structures are taken before transfer, immediately after transfer, and after a 400 °C anneal with a Nanometrics Hall mobility measurement system, while temperature-dependent Hall measurements of VdP test structures are acquired using a Lakeshore cryogenic probe station.

Conflict of Interest: The authors declare no competing financial interest.

Acknowledgment. This work was supported by the Naval Surface Warfare Center Crane, Contract No. N00164-09-C-GR34, and IRAD Project No. 01850.27. Any opinions, findings, conclusions, or recommendations expressed in this material are those of the authors and do not necessarily reflect the views of the Naval Surface Warfare Center Crane Division. Support for the WiteC Raman system, Leo 1530 SEM, Digital Instruments AFM, Kratos Axis Ultra XPS, and nanofabrication facilities was provided by the National Nanotechnology Infrastructure Network at Penn State.

REFERENCES AND NOTES

1. Novoselov, K. S.; Geim, A. K.; Morozov, S. V.; Jiang, D.; Zhang, Y.; Dubonos, S. V.; Grigorieva, I. V.; Firsov, A. A. Electric Field Effect in Atomically Thin Carbon Films. *Science* **2004**, *306*, 666–669.
2. Novoselov, K. S.; Geim, A. K.; Morozov, S. V.; Jiang, D.; Katsnelson, M. I.; Grigorieva, I. V.; Dubonos, S. V.; Firsov, A. A. Two-Dimensional Gas of Massless Dirac Fermions in Graphene. *Nature* **2005**, *438*, 197–200.
3. Shishir, R. S.; Ferry, D. K. Intrinsic Mobility in Graphene. *J. Phys.: Condens. Matter* **2009**, *21*, 232204.
4. Akturk, A.; Goldsman, N. Electron Transport and Full-Band Electron-Phonon Interactions in Graphene. *J. Appl. Phys.* **2008**, *103*, 053702.
5. Moon, J. S.; Curtis, D.; Bui, S.; Hu, M.; Gaskill, D. K.; Tedesco, J. L.; Asbeck, P.; Jernigan, G. G.; VanMil, B. L.; Myers-Ward, R. L.; *et al.* Top-Gated Epitaxial Graphene FETs on Si-Face SiC Wafers with a Peak Transconductance of 600mS/mm. *IEEE Electron Device Lett.* **2010**, *31*, 260–262.
6. Lin, Y. M.; Dimitrakopoulos, C.; Jenkins, K. A.; Farmer, D. B.; Chiu, H. Y.; Grill, A.; Avouris, P. 100-GHz Transistors from Wafer-Scale Epitaxial Graphene. *Science* **2010**, *327*, 662.
7. Farmer, D. B.; Chiu, H. Y.; Lin, Y. M.; Jenkins, K. A.; Xia, F.; Avouris, P. Utilization of a Buffered Dielectric To Achieve High Field-Effect Carrier Mobility in Graphene Transistors. *Nano Lett.* **2009**, *9*, 4474–4478.
8. Fallahazad, B.; Kim, S.; Colombo, L.; Tutuc, E. Dielectric Thickness Dependence of Carrier Mobility in Graphene with HfO_2 Top Dielectric. *Appl. Phys. Lett.* **2010**, *97*, 123105.
9. Robinson, J. A.; LaBella, M.; Trumbull, K. A.; Weng, X. J.; Cavalero, R.; Daniels, T.; Hughes, Z.; Hollander, M. J.; Fanton, M.; Snyder, D. Epitaxial Graphene Materials Integration: Effects of Dielectric Overlayers on Structural and Electronic Properties. *ACS Nano* **2010**, *4*, 2667–2672.
10. Hollander, M. J.; LaBella, M.; Hughes, Z.; Zhu, M.; Trumbull, K. A.; Cavalero, R.; Snyder, D. W.; Wang, X.; Hwang, E.; Datta, S.; *et al.* Enhanced Transport and Transistor Performance with Oxide Seeded High-k Gate Dielectrics on Wafer-Scale Epitaxial Graphene. *Nano Lett.* **2011**, *11*, 3601–3607.
11. Lee, B.; Park, S. Y.; Kim, H. C.; Cho, K. J.; Vogel, E. M.; Kim, M. J.; Wallace, R. M.; Kim, J. Conformal Al_3O_3 Dielectric Layer Deposited by Atomic Layer Deposition for Graphene-Based Nanoelectronics. *Appl. Phys. Lett.* **2008**, *92*, 203102.
12. Lin, Y. M.; Jenkins, K. A.; Valdes-Garcia, A.; Small, J. P.; Farmer, D. B.; Avouris, P. Operation of Graphene Transistors at Gigahertz Frequencies. *Nano Lett.* **2009**, *9*, 422.
13. Wang, X.; Tabakman, S. M.; Dai, H. Atomic Layer Deposition of Metal Oxides on Pristine and Functionalized Graphene. *J. Am. Chem. Soc.* **2008**, *130*, 8152.
14. Wu, Y. Q.; Ye, P. D.; Capano, M. A.; Xuan, Y.; Sui, Y.; Qi, M.; Cooper, J. A.; Shen, T.; Pandley, D.; Prakash, G.; *et al.* Top-Gated Graphene Field-Effect-Transistors Formed by Decomposition of SiC. *Appl. Phys. Lett.* **2008**, *92*, 092102.
15. Kedzierski, J.; Hsu, P. L.; Healy, P.; Wyatt, P. W.; Keast, C. L.; Sprinkle, M.; Berger, C.; de Heer, W. A. Epitaxial Graphene Transistors on SiC Substrates. *IEEE Trans. Electron Devices* **2008**, *55*, 2078–2085.
16. Chen, J. H.; Jang, C.; Xiao, S.; Ishigami, M.; Fuhrer, M. S. Intrinsic and Extrinsic Performance Limits of Graphene Devices on SiO_2. *Nat. Nanotechnol.* **2008**, *3*, 206–209.
17. Hwang, E. H.; Adam, S.; Das Sarma, S. Carrier Transport in Two-Dimensional Graphene Layers. *Phys. Rev. Lett.* **2007**, *98*, 18392–18397.
18. Ando, T. Screening Effect and Impurity Scattering in Monolayer Graphene. *J. Phys. Soc. Jpn.* **2006**, *75*, 074716.
19. Fratini, S.; Guinea, F. Substrate-Limited Electron Dynamics in Graphene. *Phys. Rev. B* **2008**, *77*, 195415.
20. Katsnelson, M. I.; Geim, A. K. Electron Scattering on Microscopic Corrugations in Graphene. *Phil. Trans. R. Soc. A* **2007**, *366*, 195–204.
21. Giovannetti, G.; Khomyakov, P.; Brocks, G.; Kelly, P.; Brink, J. V. D. Substrate-Induced Band Gap in Graphene on Hexagonal Boron Nitride: *Ab Initio* Density Functional Calculations. *Phys. Rev. B* **2007**, *76*, 073103.
22. Corso, M.; Auwarter, W.; Muntwiler, M.; Tamai, A.; Greber, T.; Osterwalder, J. Boron Nitride Nanomesh. *Science* **2004**, *303*, 217–220.
23. Paffett, M. T.; Simonson, R. J.; Papin, P.; Paine, R. T. Borazine Adsorption and Decomposition at Pt(111) and Ru(001) Surfaces. *Surf. Sci.* **1990**, *232*, 286–296.
24. Nagashima, A.; Tejima, N.; Gamou, Y.; Kawai, T.; Oshima, C. Electronic Structure of Monolayer Hexagonal Boron Nitride Physisorbed on Metal Surfaces. *Phys. Rev. Lett.* **1995**, *75*, 3918–3921.

25. Corso, M.; Breber, T.; Osterwalder, J. h-BN on Pd(110): A Tunable System for Self-Assembled Nanostructures? *Surf. Sci.* **2005**, *577*, L78–L84.
26. Preobrajenski, A. B.; Vinogradov, A. S.; Martensson, N. Monolayer of h-BN chemisorbed on Cu(111) and Ni(111): The role of the transistion metal 3d states. *Surf. Sci.* **2005**, *582*, 21–30.
27. Dean, C. R.; Young, A. F.; Meric, I.; Lee, C.; Wang, L.; Sorgenfrei, S.; Watanabe, K.; Taniguchi, T.; Kin, P.; Shepard, L.; *et al*. Boron Nitride Substrates for High-Quality Graphene Electronics. *Nat. Nanotechnol.* **2010**, *5*, 722–726.
28. Nag, A.; Raidongia, K.; Hembram, K. P. S.; Datta, R.; Waghmare, U. V.; Rao, C. N. R. Graphene Analogues of BN: Novel Synthesis and Properties. *ACS Nano* **2010**, *4*, 1539–1544.
29. Kim, E.; Yu, T.; Song, E. S.; Yu, B. CVD-Assembled Graphene Field Effect Transistors on Hexagonal Boron Nitride. *Appl. Phys. Lett.* **2011**, *98*, 262103.
30. Gannett, W.; Regan, W.; Watanabe, K.; Taniguchi, T.; Crommie, M. F.; Zetti, A. Boron Nitride Substrate for High Mobility Chemical Vapor Deposited Graphene. *Appl. Phys. Lett.* **2011**, *98*, 242105.
31. Wang, H.; Taychatanapat, T.; Hsu, A.; Watanabe, K.; Taniguchi, T.; Jarillo-Herrero, P.; Palacios, T. BN/Graphene/BN Transistors for RF Applications. *IEEE Electron Device Lett.* **2011**, *32*, 1209–1211.
32. Lee, K. H.; Shin, H.; Lee, J.; Lee, I.; Kim, G.; Choi, J.; Kim, S. Large-Scale Synthesis of High-Quality Hexagonal Boron Nitride Nanosheets for Large-Area Graphene Electronics. *Nano Lett.* **2012**, *12*, 714–718.
33. Liao, L.; Lin, Y. C.; Bao, M.; Cheng, R.; Bai, J.; Liu, Y.; Qu, Y.; Wang, K. L.; Huang, Y.; Duan, X. High-Speed Graphene Transistors with a Self-Aligned Nanowire Gate. *Nat. Lett.* **2010**, *467*, 305–308.
34. Riedl, C.; Coletti, C.; Iwasaki, T.; Zakharov, A. A.; Starke, U. Quasi-Free-Standing Epitaxial Graphene on SiC Obtained by Hydrogen Intercalation. *Phys. Rev. Lett.* **2009**, *103*, 246804.
35. Robinson, J. A.; Hollander, M.; LaBella, M.; Trumbull, K. A.; Cavalero, R.; Snyder, D. W. Epitaxial Graphene Transistors: Enhancing Performance *via* Hydrogen Intercalation. *Nano Lett.* **2011**, *11*, 3875–3880.
36. Kim, K. K.; Hsu, A.; Jia, X.; Kim, S. M.; Shi, Y.; Hofmann, M.; Nezich, D.; Rodriguez-Nieva, J. F.; Dresselhaus, M.; Palacios, T.; *et al*. Synthesis of Monolayer Hexagonal Boron Nitride on Cu Foil Using Chemical Vapor Deposition. *Nano Lett.* **2012**, *12*, 161–166.
37. Yates, B.; Overy, M. J.; Pirgon, O. The Anisotropic Thermal Expansion of Boron Nitride. *Philos. Mag.* **1975**, *32*, 847–857.
38. Li, X.; Zhu, Y.; Cai, W.; Borysiak, M.; Han, B.; Chen, D.; Piner, R. D.; Colombo, L.; Ruoff, R. S. Transfer of Large-Area Graphene Films for High-Performance Transparent Conductive Electrodes. *Nano Lett.* **2009**, *9*, 4359–4363.
39. Geick, R.; Perry, C. H. Normal Modes in Hexagonal Boron Nitride. *Phys. Rev.* **1966**, *146*, 543–547.
40. Mohiuddin, T. M. G.; Lombardo, A.; Nair, R. R.; Bonetti, A.; Savini, G.; Jalil, R.; Bonini, N.; Basko, D. M.; Galiotis, C.; Marzari, N.; *et al*. Uniaxial Strain in Graphene by Raman Spectroscopy: G Peak Splitting, Gruneisen Parameters, and Sample Orientation. *Phys. Rev. B.* **2009**, *79*, 205433.
41. Kern, G.; Kresse, G.; Hafner, J. *Ab Initio* Calculation of the Lattice Dynamics and Phase Diagram of Boron Nitride. *Phys. Rev. B.* **1999**, *59*, 8551–8559.
42. Gorbachev, R. V.; Riaz, I.; Nair, R. R.; Jalil, R.; Britnell, L.; Belle, B. D.; Hill, E. W.; Novoselov, K. S.; Watanabe, K.; Taniguchi, T.; *et al*. Hunting for Monolayer Boron Nitride: Optical and Raman Signatures. *Small* **2011**, *7*, 465–468.
43. Arenal, R.; Ferrari, A. C.; Reich, S.; Wirtz, L.; Mevellec, J. Y.; Lefrant, S.; Rubio, A.; Loiseau, A. Raman Spectroscopy of Single-Wall Boron Nitride Nanotubes. *Nano Lett.* **2006**, *6*, 1812–1816.
44. Tuinstra, F.; Koenig, J. L. Raman Spectrum of Graphite. *J. Chem. Phys.* **1970**, *53*, 1126–1131.
45. Moulder, J. F.; Stickle, W. F.; Sobol, P. E.; Bombem, D. *Handbook of X-ray Photoelectron Spectroscopy*; Chastain, J., Ed.; Perkin Elmer Co.: Eden Prairie, MN, 1992.
46. Ci, L.; Song, L.; Jin, C.; Jariwala, D.; Wu, D.; Li, Y.; Srivastava, A.; Wange, Z. F.; Storr, K.; Balicas, L.; *et al*. Atomic layers of hybridized boron nitride and graphene domains. *Nat. Mater.* **2010**, *9*, 430–435.
47. Konar, A.; Fang, T.; Jena, D. Effect of High-k Gate Dielectrics on Charge Transport in Graphene-Based Field Effect Transistors. *Phys. Rev. B.* **2010**, *82*, 115452.
48. Hollander, M. J.; Agrawal, A.; Bresnehan, M. S.; LaBella, M.; Trumbull, K. A.; Cavalero, R.; Snyder, D. W.; Datta, S.; Robinson, J. A. Unpublished work, **2012**.
49. Ristein, J.; Mammadov, S.; Seyller, Th. The Origin of Doping in Quasi-Free Standing Graphene on Silicon Carbide. *Condens. Mater.* **2011**, arXiv:1109.6907.
50. Robinson, J. A.; Trumbull, K. A.; LaBella, M.; Cavalero, R.; Hollander, M. J.; Zhu, M.; Wetherington, M. T.; Fanton, M.; Snyder, D. W. Effects of Substrate Orientation on the Structural and Electronic Properties of Epitaxial Graphene on SiC(0001). *Appl. Phys. Lett.* **2011**, *98*, 222109.
51. Farmer, D.; Perebeinos, V.; Lin, Y.; Dimitrakopoulos, C.; Avouris, P. Charge Trapping and Scattering in Epitaxial Graphene. *Phys. Rev. B.* **2011**, *84*, 205417.
52. Britnell, L.; Gorbachev, R. V.; Jalil, R.; Belle, B. D.; Schedin, F.; Katsnelson, M. I.; Eaves, L.; Morozov, S. V.; Mayorov, A. S.; Peres, L. A. Electron Tunneling Through Ultrathin Boron Nitride Crystalline Barriers. *Nano Lett.* **2012**, *12*, 1707–1710.
53. Robinson, J. A.; LaBella, M.; Zhu, M.; Hollander, M.; Kasarda, R.; Hughes, Z.; Trumbull, K.; Cavalero, R.; Snyder, D. Contacting Graphene. *Appl. Phys. Lett.* **2011**, *98*, 053103.
54. Song, L.; Ci, L.; Lu, H.; Sorokin, P. B.; Jin, C.; Ni, J.; Kvashnin, A. G.; Kvashnin, D. G.; Lou, J.; Yakobson, B. I.; *et al*. Large Scale Growth and Characterization of Atomic Hexagonal Boron Nitride Layers. *Nano Lett.* **2010**, *10*, 3209–3215.
55. Li, X.; Cai, W.; An, J.; Kim, S.; Nah, J.; Yang, D.; Piner, R.; Velamakanni, A.; Jung, I.; Tutuc, E.; *et al*. Large-Area Synthesis of High-Quality and Uniform Graphene Films on Copper Foils. *Science* **2009**, *324*, 1312–1314.